

# Gravity Waves in a Horizontal Shear Flow. Part I: Growth Mechanisms in the Absence of Potential Vorticity Perturbations

NIKOLAOS A. BAKAS AND BRIAN F. FARRELL

*Harvard University, Cambridge, Massachusetts*

(Manuscript received 7 May 2007, in final form 17 July 2008)

## ABSTRACT

Interaction of internal gravity waves with a horizontal shear flow in the absence of potential vorticity perturbations is investigated making use of closed-form solutions. Localized wave packet trajectories are obtained, the energy growth mechanisms occurring are identified, and the potential role of perturbation growth in wave breaking is assessed.

Regarding meridional propagation, the wave packet motion is limited by turning levels where the waves are reflected and trapping levels where the waves stagnate. Regarding perturbation energy amplification, two growth mechanisms can be distinguished: growth due to advection of zonal velocity and growth due to downgradient Reynolds stresses. The three-dimensional perturbations producing optimal energy growth reveal that these two mechanisms produce large and robust amplification of zonal velocity and/or density and vertical velocity, potentially leading to shear or convective instability.

For large static stability, amplification of density perturbations in conjunction with vertical orientation of the constant phase lines close to the trapping level potentially leads to a convective collapse of the wave packet near the trapping level, in agreement with existing direct numerical simulation studies. For lower static stability and for waves with phase lines oriented horizontally, growth due to advection of zonal velocity dominates, leading to rapid growth of streamwise streaks within the localized wave packet and potentially to shear instability.

## 1. Introduction

One of the important roles of the internal gravity wave field is its contribution to oceanic small-scale mixing. Even though there have been a large number of attempts to quantify the rates at which the internal wave field produces mixing in the ocean (for reviews, see Garrett and Munk 1979; Gregg 1989; Staquet and Sommeria 2002), we still lack an adequate understanding of both the sources of internal wave energy and the rate at which it is dissipated. Mechanisms of gravity wave generation and growth leading to breaking are examined in this work by studying the evolution of small perturbations in a stably stratified, horizontally sheared flow. In this first part, we concentrate on the interaction of gravity waves with shear, while in the companion paper (Bakas and Farrell 2009, hereafter Part II) the

focus is on the interaction between potential vorticity perturbations and gravity waves.

Interaction of internal gravity waves with horizontally inhomogeneous oceanic currents has been investigated observationally (Frankignoul 1974; Ruddick and Joyce 1979) and experimentally (Thorpe 1981). Theoretical studies addressing this problem typically employ a linear analysis and the Wentzel–Kramers–Brillouin (WKB) approximation (Bretherton 1966; Olbers 1981; Badulin and Shrira 1993) or a weakly nonlinear analysis (Brown and Stewartson 1982). For example, Samodurov (1974) and Miropol'skiy (1974) considered the effect of a vertically constant but horizontally varying buoyancy frequency on internal wave propagation. They found that waves are trapped near locations where the intrinsic frequency approaches the Brunt–Väisälä frequency, analogous to the trapping by a critical level in a vertical shear. Analogous behavior of gravity waves near trapping levels will be a focal point of this study as well.

Internal wave trapping in a baroclinic shear flow that is in thermal wind balance with a horizontal density gradient in a stably stratified fluid was studied by Olbers

---

*Corresponding author address:* Nikolaos Bakas, National and Kapodistrian University of Athens, Office 32, Build IV, Panepistimiopolis, Zografos, Athens, Greece.  
E-mail: nikos.bakas@gmail.com

(1981). He showed using the WKB approximation that wave energy focuses at depths where Brunt–Väisälä frequency maxima occur, and evidence for such a trapping mechanism in the Lomonosov Current was provided by Badulin et al. (1990). Olbers (1981) further showed that as a wave approaches its trapping level, both its wavelength and group velocity in the direction of the inhomogeneity decay to zero. Consequently, the wave vector approaches the horizontal inhomogeneity direction and the intrinsic frequency tends to the Brunt–Väisälä frequency. The trapping level is never reached in the WKB limit, and both wave amplitude and wave energy density increase without bound in the inviscid limit. These conclusions were confirmed by exact solutions of the model problem (Erokhin and Sagdeev 1985).

Further insight into wave behavior near the trapping level was obtained by linearizing about a barotropic horizontal parallel shear flow (Ivanov and Morozov 1974). For a wave train, concentration of wave energy due to group velocity reduction near the trapping level results in a local energy growth leading to breaking (Badulin et al. 1990). Staquet and Huerre (2002), using direct numerical simulations of an inertia–gravity wave packet approaching a dynamical barrier, verified that breaking is possible in the trapping plane neighborhood even for a wave packet. However, they found that breaking is caused by an increase in density and vertical velocity that cannot be attributed to wave packet energy accumulation. Because breaking occurred regardless of whether the flow supported exponential instabilities, this result links wave breaking to transient nonnormal growth. Such algebraic growth was found by Kalashnik et al. (2006) in numerical integrations of the linearized equations governing the evolution of small perturbations in a meridionally varying shear flow on an  $f$  plane.

Because breaking of gravity waves near the trapping level occurs regardless of rotational effects, the Coriolis acceleration will be neglected in this work. Instead, we focus on an inertial frame of reference and extend the analysis of Kalashnik et al. (2006), identifying all the transient growth mechanisms occurring and investigating, in addition, their role in wave breaking. To achieve this goal, we use the tools provided by the generalized stability theory (GST) developed by Farrell and Ioannou (1996), a mathematical framework for addressing transient perturbation growth. We perform a generalized stability analysis of a linear three-dimensional model with a barotropic horizontal shear flow  $\mathbf{U} = U(y)\hat{i}$  and a constant Brunt–Väisälä frequency. In this first part, we consider an unbounded constant shear flow allowing closed-form solutions to the initial value problem and investigate the problem of wave packet propagation and

mean flow interaction for perturbations without initial potential vorticity. We also find the structures that amplify most in energy and discuss the implications of these optimal structures for wave breaking. In Part II, we study the interaction between vorticity perturbations and internal gravity waves.

This paper is organized as follows: in section 2, we describe the linear evolution equations for perturbations in a stratified, barotropic horizontal shear flow. Sections 3 and 4 describe the growth mechanism and propagation of zonally independent perturbations and of perturbations in the strong stratification limit, respectively. The synergy between the two mechanisms for growth is studied in section 5, while the optimal growing perturbations are identified in section 6. The intuition gained and the analytical results obtained are used in section 7 to study the interaction of localized wave packets with the shear flow. We finally end with a brief discussion and our conclusions in section 8.

## 2. Formulation

### a. Evolution equations for three-dimensional perturbations

Consider a flow with mean zonal velocity  $U(y)$  varying only in the meridional direction in a hydrostatically balanced, stratified ocean of background density  $\rho = \rho_m + \rho_0(z)$ , where  $\rho_m$  is the mean density and  $\rho_0(z)$  is the variation of the background density with depth. Velocity perturbations superposed on the background flow in the zonal, meridional, and vertical direction are  $(u, v, w)$ , respectively. Density and pressure perturbations superposed on the mean density and pressure fields are  $(\rho, p)$ , respectively. The linearized, nondimensional momentum, thermodynamic, and continuity equations governing the evolution of small perturbations are

$$(\partial_t + U(y)\partial_x)u + \frac{dU}{dy}v = -\partial_x p - r(y)u + \frac{1}{\text{Re}}\nabla^2 u, \quad (1)$$

$$(\partial_t + U(y)\partial_x)v = -\partial_y p - r(y)v + \frac{1}{\text{Re}}\nabla^2 v, \quad (2)$$

$$(\partial_t + U(y)\partial_x)w = -\partial_z p - S\rho - r(y)w + \frac{1}{\text{Re}}\nabla^2 w, \quad (3)$$

$$(\partial_t + U(y)\partial_x)\rho = \frac{N^2}{N_0^2}w - r(y)\rho + \frac{1}{\text{Re}}\nabla^2 \rho, \quad (4)$$

$$\partial_x u + \partial_y v + \partial_z w = 0. \quad (5)$$

Time is nondimensionalized by  $1/\alpha$ , where  $\alpha$  is the shear and the horizontal and vertical scales are nondimensionalized by  $L = V_0/\alpha$ , where  $V_0$  is a typical

mean flow velocity. Pressure and density are non-dimensionalized by  $\rho_m V_0^2$  and  $\rho_m V_0 N_0^2 / \alpha g$ , respectively, where  $g$  is the gravitational acceleration and  $N_0$  is a characteristic value of the Brunt–Väisälä frequency. The Brunt–Väisälä frequency  $N$ , defined as  $N^2 = -(g/\rho_m)(d\rho_0/dz)$ , is constant and taken to be equal to its characteristic value  $N^2 = N_0^2$ . The nondimensional static stability and the Reynolds number are defined as  $S = N_0^2/\alpha^2$  and  $Re = \rho_m L V_0/\mu$ , respectively, where  $\mu$  is the coefficient of viscosity. The Prandtl number has been chosen to be one, thus the coefficient of kinematic viscosity  $\nu = \mu/\rho_m$  equals the coefficient of density diffusion. The Rayleigh damping terms  $r(y)$  are only relevant to the numerical calculations presented in Part II, where further details will be provided.

We first take advantage of the continuity equation to reduce the number of partial differential equations to three. Taking the divergence of momentum Eqs. (1), (2), and (3), and using continuity equation (5), we obtain the diagnostic equation for the perturbation pressure:

$$\nabla^2 p = -2 \frac{dU}{dy} \partial_x v - \frac{dr}{dy} v - S \partial_z \rho. \tag{6}$$

Eliminating pressure from (1), (3) we obtain the evolution equation for the meridional component of vorticity  $\zeta = \partial_z u - \partial_x v$ :

$$\left( \partial_t + U \partial_x + r - \frac{1}{Re} \nabla^2 \right) \zeta = - \frac{dU}{dy} \partial_z v + S \partial_x \rho. \tag{7a}$$

Applying the Laplacian operator to (2) and eliminating pressure using (6) yields

$$\left( \partial_t + U \partial_x + r - \frac{1}{Re} \nabla^2 \right) \nabla^2 v = \left( \frac{d^2 U}{dy^2} \partial_x - \frac{dr}{dy} \partial_y \right) v + S \partial_{yz}^2 \rho. \tag{7b}$$

Finally, applying the operator  $(\partial_x^2 + \partial_z^2)$  to (4) and using continuity equation (5) and the definition of  $\zeta$  yields

$$\left( \partial_t + U \partial_x + r - \frac{1}{Re} \nabla^2 \right) (\partial_x^2 + \partial_z^2) \rho = - \partial_x \zeta - \partial_{yz}^2 v. \tag{7c}$$

We thus obtain the system (7) that determines the evolution of the meridional component of vorticity  $\zeta$ , meridional component of velocity  $v$ , and perturbation density  $\rho$ .

*b. Perturbation dynamics in the convected frame of reference*

Consider an inviscid, unbounded, constant shear flow  $U(y) = y$  in the absence of Rayleigh damping ( $r = 0$ ). It is

useful to transform system (7) into the convected coordinate frame of reference (Phillips 1966), which is moving with the background flow ( $\xi = x - yt$ ), and seek solutions of the form  $[\zeta, v, \rho] = [\hat{\zeta}(t), \hat{v}(t), \hat{\rho}(t)] e^{ikx + i(l-kt)y + imz}$  with time-varying meridional wavenumber  $l - kt$ . Substituting this solution form reduces the original partial differential equations to the following set of three ordinary differential equations:

$$\frac{d\hat{\zeta}}{dt} = -im\hat{v} + ikS\hat{\rho} - \frac{K(t)^2}{Re} \hat{\zeta}, \tag{8a}$$

$$\frac{d\hat{v}}{dt} = \frac{2k(l-kt)}{K(t)^2} \hat{v} + \frac{m(l-kt)S}{K(t)^2} \hat{\rho} - \frac{K(t)^2}{Re} \hat{v}, \tag{8b}$$

$$\frac{d\hat{\rho}}{dt} = \frac{ik}{k^2 + m^2} \hat{\zeta} - \frac{m(l-kt)}{k^2 + m^2} \hat{v} - \frac{K(t)^2}{Re} \hat{\rho}, \tag{8c}$$

where  $K(t)^2 = k^2 + m^2 + (l - kt)^2$  is the square of the time-dependent total wavenumber of the plane wave. Even though (8) is a self-contained system and its solution can be accurately determined by numerical integration, it is instructive to reduce it to a single second-order differential equation by taking advantage of potential vorticity conservation for an inviscid flow, as this separates the growth processes considered in this study from growth processes due to gravity wave–vorticity wave interaction considered in Part II. We first use the continuity equation (5) and the definition of  $\zeta$  to express the vertical component of potential vorticity  $q = \partial_x v - \partial_y u + \partial_z \rho$  of a single Fourier component in terms of  $\hat{\zeta}$ ,  $\hat{v}$ , and  $\hat{\rho}$ :

$$\hat{q} = \left[ - \frac{m(l-kt)}{k^2 + m^2} \hat{\zeta} + \frac{ikK(t)^2}{k^2 + m^2} \hat{v} + im\hat{\rho} \right].$$

It can be readily shown from (8) that

$$\hat{q}(t) = \hat{q}(0) e^{-(1/Re)t} \int_0^t K(s)^2 ds. \tag{9}$$

Combining Eqs. (8b), (8c), and (9), we obtain the second-order differential equation for  $\hat{\rho}$ :

$$\begin{aligned} \frac{d^2 \hat{\rho}}{dt^2} + \left\{ S\omega(t)^2 + ka(t) + \frac{K(t)^4}{Re^2} \right. \\ \left. + \frac{(l-kt)}{Re} [a(t)K(t)^2 - 2k] \right\} \hat{\rho} \\ + \left[ (l-kt)a(t) + \frac{2K(t)^2}{Re} \right] \frac{d\hat{\rho}}{dt} = - \frac{ika(t)}{m} \hat{q}(t), \tag{10} \end{aligned}$$

where

$$a(t) = \frac{2km^2}{[k^2 + (l - kt)^2]K(t)^2}, \quad (11)$$

$$\omega(t)^2 = \frac{k^2 + (l - kt)^2}{K(t)^2}. \quad (12)$$

The solution of the homogeneous restriction of (10) consists of transient gravity waves, whereas the particular solution involves the interaction between the propagating gravity waves and potential vorticity perturbations. It is therefore instructive to study the solution to the homogeneous restriction of (10) and the particular solution separately. In this work we concentrate on the solution of the homogeneous equation; that is, we hereafter consider only perturbations with  $\hat{q}(0) = 0$ . The particular solution along with the interaction between vorticity perturbations and gravity waves is studied in Part II.

### c. Perturbation energy density and energetics

To understand the transient growth mechanisms, we consider the transfers of energy between waves and the mean flow. The perturbation energy density, defined as  $E = (1/4)(\overline{u^2 + w^2 + v^2}) + (S/4)\overline{\rho^2}$ , evolves according to

$$\begin{aligned} \frac{dE}{dt} &= \frac{dT}{dt} + \frac{dV}{dt} = (-\overline{uw} - S\overline{\rho w}) + (S\overline{\rho w}) \\ &\quad - \frac{1}{\text{Re}} [\overline{(\nabla u)^2} + \overline{(\nabla v)^2} + \overline{(\nabla w)^2} + S\overline{(\nabla \rho)^2}] = \\ &\quad - \overline{uw} - \frac{1}{\text{Re}} [\overline{(\nabla u)^2} + \overline{(\nabla v)^2} + \overline{(\nabla w)^2} + S\overline{(\nabla \rho)^2}], \end{aligned} \quad (13)$$

where  $T = (1/4)\overline{(u^2 + w^2 + v^2)}$ ,  $V = (S/4)\overline{\rho^2}$  are the kinetic and potential energy density, respectively, and the overbar denotes an average over space. Therefore, perturbation energy grows due to the downgradient Reynolds stress term  $\overline{uw}$ . Note that even though the buoyancy flux term  $\overline{\rho w}$  does not contribute to net energetics, it is responsible for energy exchange between the kinetic and potential forms.

Before we treat the evolution of three-dimensional perturbations, it is instructive to consider two separate limits permitting closed-form solutions and illuminating the basic growth mechanisms in shear flow as well as the propagation characteristics of wave packets.

### 3. Growth of zonally independent solutions

Consider first the limit of zonally uniform solutions ( $k = 0$ ) in an inviscid flow. The Lagrangian zonal velocity of these roll solutions is conserved (Moffat 1967;

Ellingsen and Palm 1975; Landahl 1980). Such perturbations can therefore grow by advection of mean zonal velocity by perturbation spanwise velocity to regions of lower/higher mean zonal velocity. For an unstratified flow, the vertical and meridional perturbation velocities are constant, leading to a continuous advection and to linear growth of zonal velocity (Farrell and Ioannou 1993).

In the presence of stratification, vertical motion is opposed by the buoyancy force, and growth of roll perturbations in a vertical shear is limited by stratification to  $E O(1/\text{Ri})$  (Bakas et al. 2001). For roll perturbations in a stratified meridional shear, meridional and vertical velocities satisfy the continuity equation  $v = -(m/l)w$ . Therefore, for large  $m/l$ —that is, if the phase lines are almost horizontal—a small vertical motion will correspond to large meridional advection of zonal velocity leading to large zonal velocity growth. The solution of (10) for the time-dependent Fourier components in this case is

$$\begin{aligned} \hat{\zeta}(t) &= \frac{1}{2} \left[ \frac{im^2}{l} \hat{\rho}(0) - \frac{m}{\omega_0} \hat{v}(0) \right] e^{i\omega_0 t} \\ &\quad + \frac{1}{2} \left[ \frac{im^2}{l} \hat{\rho}(0) + \frac{m}{\omega_0} \hat{v}(0) \right] e^{-i\omega_0 t}, \end{aligned} \quad (14)$$

$$\begin{aligned} \hat{v}(t) &= \frac{1}{2} \left[ \hat{v}(0) + \frac{m\omega_0}{il} \hat{\rho}(0) \right] e^{i\omega_0 t} \\ &\quad + \frac{1}{2} \left[ \hat{v}(0) - \frac{m\omega_0}{il} \hat{\rho}(0) \right] e^{-i\omega_0 t}, \end{aligned} \quad (15)$$

$$\begin{aligned} \hat{\rho}(t) &= \frac{1}{2} \left[ \hat{\rho}(0) - \frac{l}{im\omega_0} \hat{v}(0) \right] e^{i\omega_0 t} \\ &\quad + \frac{1}{2} \left[ \hat{\rho}(0) + \frac{l}{im\omega_0} \hat{v}(0) \right] e^{-i\omega_0 t}, \end{aligned} \quad (16)$$

where

$$\omega_0 = l\sqrt{S}/\sqrt{l^2 + m^2}, \quad (17)$$

yielding the general solution

$$\begin{aligned} &[\hat{\zeta}(y, z, t), \hat{v}(y, z, t), \hat{\rho}(y, z, t)] \\ &= \frac{1}{2\pi} \int_{-\infty}^{\infty} \int_{-\infty}^{\infty} [\hat{\zeta}(t), \hat{v}(t), \hat{\rho}(t)] e^{imz + ily} dldm, \end{aligned} \quad (18)$$

where

$$\begin{aligned} &[\hat{\zeta}(0), \hat{v}(0), \hat{\rho}(0)] = \frac{1}{2\pi} \int_{-\infty}^{\infty} \int_{-\infty}^{\infty} [\hat{\zeta}(y, z, t = 0), \\ &v(y, z, t = 0), \rho(y, z, t = 0)] e^{-ily - imz} dydz. \end{aligned}$$

All Fourier components oscillate with the frequency,  $\omega_0$  satisfying the dispersion relation of a gravity wave in the  $(y, z)$  plane. The two terms in (14)–(16) therefore represent

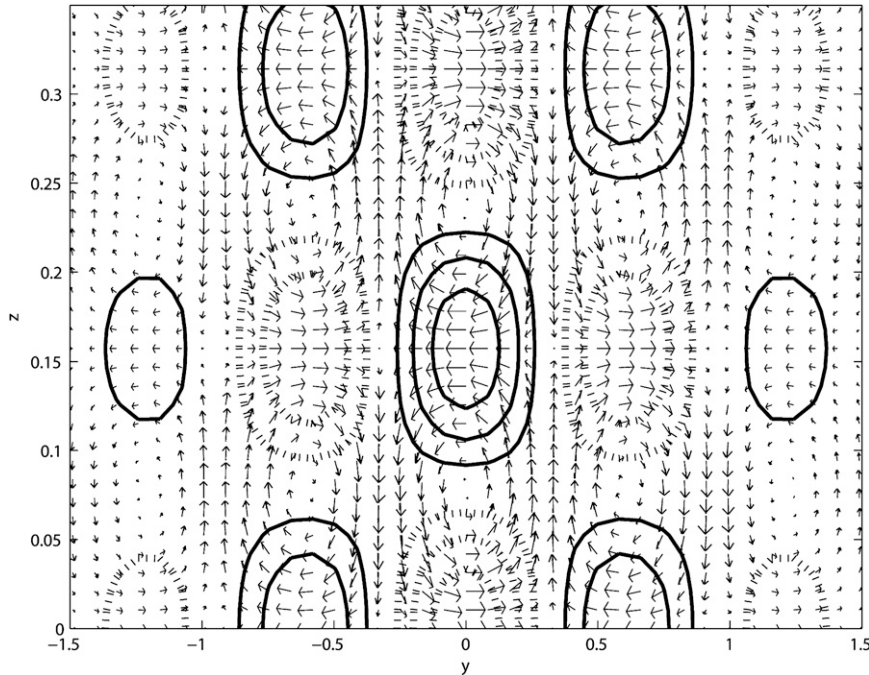


FIG. 1. Structure at  $t = 2$  of the wave packet with initial structure  $v(y, z, t = 0) = A_v e^{-y^2/(\delta y)^2} \cos(mz) \cos(l y)$ . Shown are the velocity field in the  $(y, z)$  plane (vectors) and zonal velocity,  $u$  (contours). The contour interval is  $1/2$  and negative values are dashed. Static stability is  $S = 1$ ,  $(l, m) = (5, 20)$ ,  $\delta y = 1.25$ , and  $A_v$  is such that the initial wave packet has unit energy. Formation of zonal velocity perturbations potentially leading to shear instability is a prominent feature of this solution.

two counterpropagating waves in the  $(y, z)$  plane. The structure and evolution of an initial localized perturbation  $v(y, z, t = 0) = A_v e^{-y^2/(\delta y)^2} \cos(mz) \cos(l y)$ , where  $A_v$  is a chosen amplitude, are calculated using numerical quadrature of the Fourier integral (18) and are shown in Figs. 1, 2. This localized initial perturbation consists of a roll type of circulation in the  $(y, z)$  plane (Fig. 1) with meridional velocity leading zonal velocity by a quarter of a wavelength in the vertical, and it subsequently evolves as two counterpropagating coherent wave packets.

Its energy evolution found by numerical quadrature of the Fourier integral

$$E(t) = \frac{1}{8\pi} \int_{-\infty}^{\infty} \int_{-\infty}^{\infty} \frac{1}{m^2} [|\hat{\xi}(t)|^2 + (l^2 + m^2)|\hat{v}(t)|^2 + S m^2 |\hat{\rho}(t)|^2] dldm \tag{19}$$

is plotted in Fig. 2. Initially, an oscillation due to wave interference is observed, but as the counterpropagating wave packets separate in space (Fig. 2), the energy asymptotes to a constant large value. Further investigation of (19) reveals that this energy growth can be traced to zonal velocity growth due to roll advection as de-

scribed in the beginning of this section. This observation suggests that roll perturbations propagating within a shear region can produce large streamwise velocity perturbations that may lead to breaking through shear instability. It is therefore of interest to identify the perturbations leading to the largest energy growth both

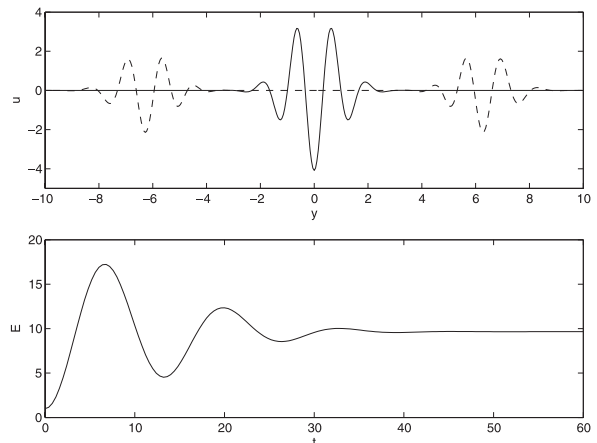


FIG. 2. Evolution of the wave packet shown in Fig. 1. (top) Real part of zonal velocity  $u$  at  $z = 0$  for  $t = 6.5$  (solid line) and  $t = 136$  (dashed line). (bottom) Energy of the wave packet as calculated by numerical quadrature of (19).

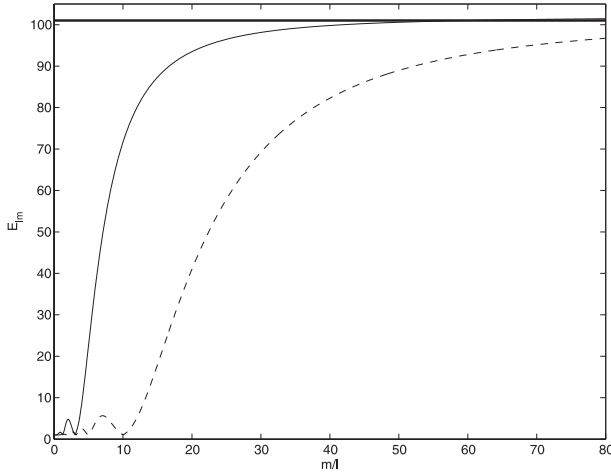


FIG. 3. The maximum energy growth  $E_{lm}^m$  given by (A2) as a function of  $m/l$  for static stability  $S = 1$  (solid line) and  $S = 10$  (dashed line). The optimizing time is  $T_{\text{opt}} = 10$  and the upper bound  $1 + T_{\text{opt}}^2$  is shown by the thick line.

during the initial evolution when there is wave interference and at the final stage of wave spatial separation. The maximum growth that can be achieved provides a measure of the strength of the growth mechanism due to advection, and the optimal perturbations identify the structures that are expected to dominate perturbation dynamics in the linear limit and to develop regions susceptible to wave breaking.

In appendix A we obtain closed-form solutions for the optimal roll perturbations maximizing energy growth at a specified time  $T_{\text{opt}}$ , which can be chosen to be within the time interval either of wave interference or wave spatial separation. That is, for a plane wave perturbation of given wavenumbers,  $(l, m)$ , we calculate the initial conditions leading to maximum energy  $E_{\text{opt}}^{lm}(T_{\text{opt}})$  at the specified time  $T_{\text{opt}}$  under the constraint of unit initial energy. The optimal perturbations are then obtained by calculating the wavenumbers  $(l, m)$  maximizing  $E_{\text{opt}}^{lm}$ . In the case of wave interference, the energy growth  $E_{\text{opt}}^{lm}$  given by (A2) is plotted in Fig. 3 as a function of  $m/l$  for  $S = 1$  and  $S = 20$ . Apart from local minima and maxima for low values of the tilt  $m/l$ , growth increases and asymptotes to approximately  $T_{\text{opt}}^2$  for  $m/l \rightarrow \infty$ , as meridional advection for a given vertical motion is maximized when the phase lines are almost horizontal. The optimal initial perturbations producing this growth for  $m/l \rightarrow \infty$  are velocity perturbations. Also note that even though the optimal growth is obtained for perturbations having  $m/l$  tending to infinity in the inviscid limit, 90% of the maximum growth  $E_{\text{opt}}^{lm}$  is reached at  $m/l \sim 15\sqrt{S}$ . Therefore, in realistic viscous flows in which diffusion attenuates short wavelength disturbances, the roll mechanism is expected to be more

effective for lower static stability. In the case of wave spatial separation, the optimal perturbations have again almost horizontal phase lines ( $m/l \gg 1$ ) and the optimal initial conditions are velocity perturbations leading to an overall energy increase of  $E_{\text{opt}}^{lm} \sim 1 + m^2/(2l^2S)$ , which is independent of the optimization time (as long as this is chosen to be within the time interval of wave spatial separation). In summary, growth of zonal velocity due to roll advection is larger for low static stability and for nearly horizontal initial velocity perturbations.

#### 4. Growth of perturbations in the strong stratification limit

We now investigate the energy growth and propagation properties of perturbations varying weakly in the vertical. Consider Eq. (10) in the absence of diffusion:

$$\frac{d^2 \hat{\rho}}{dt^2} + (l - kt)a(t) \frac{d\hat{\rho}}{dt} + [S\omega(t)^2 + ka(t)]\hat{\rho} = 0. \quad (20)$$

The leading large time asymptotic behavior of perturbations is easily determined. The horizontal velocity components decay to zero, while vertical velocity and density oscillate with the nondimensional Brunt–Väisälä frequency ( $\hat{w}, \hat{\rho}$ )  $\sim e^{\pm i\sqrt{S}t}$ , indicating the existence of a trapping level, as discussed in the introduction. Introducing  $\tilde{\rho}(t) = \hat{\rho}(t)\omega(t)$  and reorganizing terms in (20), we obtain

$$\frac{d^2 \tilde{\rho}}{dt^2} + Q(t)\tilde{\rho} = 0, \quad (21)$$

where

$$Q(t) = S\omega(t)^2 + \frac{k^2 m^2 [3k^2(k^2 + m^2) + 2k^2(l - kt)^2 - (l - kt)^4]}{[k^2 + (l - kt)^2]^2 [k^2 + m^2 + (l - kt)^2]^2}. \quad (22)$$

For  $(m/k) \ll S^{1/2}$ ,  $Q$  is a slowly varying function of time  $\{|Q'/Q^{3/2}|O[(m/k)/S^{1/2}] \ll 1\}$  and a WKB analysis can be applied to (21). The WKB solution to (21) is

$$\tilde{\rho} = Q(t)^{-1/4} e^{\pm i \int_0^t \sqrt{Q(s)} ds}. \quad (23)$$

For  $(m/k) \ll S^{1/2}$ ,  $Q(t) = S\omega(t)^2 + O[(m/k)/S^{1/2}]$ , and (23) reduces to

$$\begin{aligned} \hat{\rho} &= \omega(t)Q(t)^{-1/4} e^{\pm i \int_0^t \sqrt{Q(s)} ds} \\ &= S^{-1/4} \sqrt{\omega(t)} e^{\pm i\sqrt{S} \int_0^t \omega(s) ds} + O[(m/k)/S^{1/2}]. \end{aligned} \quad (24)$$

We define  $F = (m/k)/S^{1/2}$  as an inverse stratification parameter that also depends on the vertical orientation of perturbations. Therefore, for  $(m/k) \ll S^{1/2}$  ( $F \ll 1$ ), the solution consists of internal gravity waves with time-dependent meridional wavenumber  $\tilde{l} = l - kt$  and time-dependent Doppler-shifted frequency  $\sqrt{S}\omega(t)$ , satisfying the internal wave dispersion relation with the instantaneous value of the time-dependent meridional wavenumber. The approximate solution (24) to  $O(F)$  is remarkably accurate for  $F < 0.3$ , whereas for  $F \sim O(1)$  the relative error is around 30%.

Consider now a wave packet of initial perturbations consisting of a spread  $\Delta l$  of wave vectors about a central vector  $l_0$  subject to  $|\Delta l|/|l_0| \ll 1$ . We calculate in appendix B the solution for such a localized perturbation along with the evolution of its group velocity and energy. We show that the initial perturbation evolves into two counterpropagating coherent wave packets, whose meridional displacement and group velocity as a function of time are

$$\hat{y}(t) = \hat{y}(0) \pm \frac{\sqrt{S}}{k_0} [\omega(l_0, t) - \omega(l_0, 0)], \tag{25}$$

$$c_{g_y} = \frac{d\hat{y}}{dt} = \frac{\pm m_0^2(l_0 - k_0 t)\sqrt{S}}{[k_0^2 + (l_0 - k_0 t)^2]^{1/2} [k_0^2 + m_0^2 + (l_0 - k_0 t)^2]^{3/2}}, \tag{26}$$

where the plus and minus signs correspond to the two counterpropagating wave packets.

From (25) and (26) we can see that under the assumption of a positive zonal wavenumber  $k_0$ , an initial disturbance with positive central meridional wavenumber  $l_0$  propagates northward (southward) for times  $t < l_0/k_0$ , reaching the maximum (minimum) latitude

$$\hat{y}_{\max} = \pm \frac{\sqrt{S}}{k_0} \left( \frac{k_0}{\sqrt{k_0^2 + m_0^2}} - \sqrt{\frac{k_0^2 + l_0^2}{k_0^2 + m_0^2 + l_0^2}} \right),$$

then the motion reverses and the packet asymptotically approaches the latitude

$$\hat{y}_{\infty} = \pm \frac{\sqrt{S}}{k_0} \left( 1 - \sqrt{\frac{k_0^2 + l_0^2}{k_0^2 + m_0^2 + l_0^2}} \right), \tag{27}$$

southward (northward) of its original position. On the other hand, an initial disturbance with negative  $l_0$  propagates southward (northward) all the way to the minimum (maximum) latitude of (27). The trajectory of the center of the wave packet for both cases is shown in Fig. 4.

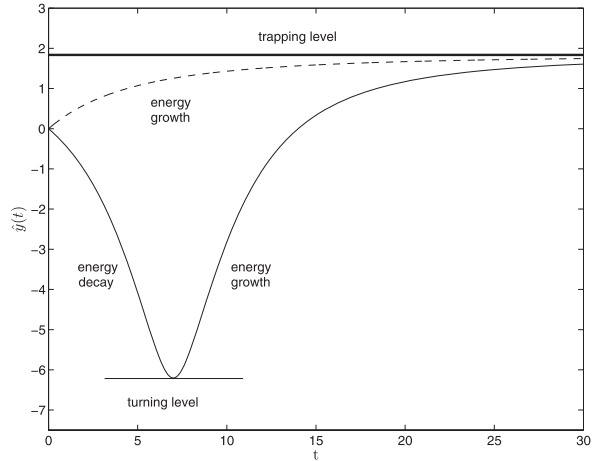


FIG. 4. Location of the center of the wave packet  $\hat{y}(t)$  [given by (25)] with time. Static stability is  $S = 100$  and the central wavenumber is  $(k_0, l_0, m_0) = (1, 7, 5)$  (solid line) and  $(k_0, l_0, m_0) = (1, -7, 5)$  (dashed line). The thick solid line denotes the trapping level for both cases, and the trajectory segments in which energy amplification and decay occur are also noted. Only the path of one of the two counterpropagating wave packets is shown [the one corresponding to the plus sign in (25)]. The path of the other wave packet is the one shown here, only reflected about the  $y = 0$  axis.

The ultimate wave packet latitudinal displacement  $\hat{y}_{\infty}$  coincides with the trapping level of a monochromatic wave with wavenumber  $\mathbf{k}_0 = (k_0, l_0, m_0)$ . If  $y_{il}$  is the distance of the wave packet from the trapping level, it is easily shown by using (25), (27) that  $\tilde{l} = l - kt \sim y_{il}^{-1/2}$  and  $c_{g_y} \sim y_{il}^{3/2}$  as  $y_{il} \rightarrow 0$ . Similarly, if  $y_{rl}$  is the distance of the wave packet from the turning level, it can be shown that  $\tilde{l} = l - kt \sim y_{rl}^{1/2}$  and  $c_{g_y} \sim y_{rl}^{1/2}$  as  $y_{rl} \rightarrow 0$ . We have thus recovered the results reported in Staquet and Huerre (2002), who used the ray-tracing method in the WKB limit. Note, however, that the approximation to (20) for  $F \ll 1$  and, consequently, the wave packet analysis does not fail near the turning point, in contrast to the WKB theory used in the ray-tracing method that becomes invalid near the turning level. Finally, it is worth noting that internal waves can propagate beyond their turning level due to nonlinear interactions between waves and wave-induced flow (Sutherland 2000), an effect that is not accounted for in our linearized analysis.

The wave packet energy evolves according to (see appendix B for details)

$$\frac{E(t)}{E(0)} = \frac{\omega(l_0, t)}{\omega(l_0, 0)} = \left\{ \frac{(k_0^2 + m_0^2 + l_0^2)[k_0^2 + (l_0 - kt)^2]}{(k_0^2 + l_0^2)[k_0^2 + m_0^2 + (l_0 - kt)^2]} \right\}^{1/2}. \tag{28}$$

For an initial positive  $l_0/k_0$ , the Reynolds stress  $\overline{uv}$  is upgradient up to time  $t_v = l_0/k_0$ , when the packet

reaches its turning level. Consequently, because the energy evolves according to (13), we have energy decay during northward/southward propagation. For later times  $t > t_v$ , the Reynolds stress is downgradient, leading to energy growth. On the other hand, for a negative  $l_0/k_0$ , the Reynolds stress is downgradient and we have monotonic energy growth during the whole time of propagation. The phases of energy amplification and decay are also noted in Fig. 4. In both cases we have energy growth as the wave packet approaches the trapping level (for  $t \rightarrow \infty$ ) and its energy asymptotes to a constant value

$$\frac{E(t)}{E(0)} \rightarrow \sqrt{1 + \frac{m_0^2}{k_0^2 + l_0^2}},$$

which is larger than its initial energy. Because almost all of the growth attained is due to density and vertical velocity amplification, it may lead to convectively unstable regions and wave breaking. We assess here the possibility of breaking of three-dimensional perturbations. We consider the ratio of maximum perturbation density gradient measured by  $n^2 = -(g/\rho_m)|\partial\rho/\partial z|$  to the background Brunt-Väisälä  $N_0^2 = -(g/\rho_m)d\rho_0/dz$ , which is given by

$$\frac{n^2}{N_0^2} = |m_0\hat{\rho}|.$$

Convective overturning may occur whenever  $n^2/N_0^2 > 1$ . The largest density amplification occurs near the trapping level and leads to

$$\begin{aligned} \frac{n^2}{N_0^2} = |m_0\hat{\rho}| &= \left| \sqrt{\frac{\omega(l_0, t \rightarrow \infty)}{\omega(l_0, 0)}} m_0\hat{\rho}(x, z, y, 0) \right| \\ &= \left| \left( 1 + \frac{m_0^2}{k_0^2 + l_0^2} \right)^{1/4} m_0\hat{\rho}(x, z, y, 0) \right|. \end{aligned}$$

We observe that for a given initial perturbation amplitude, WKB theory to  $O(F)$  predicts that perturbations with phase lines oriented almost horizontally are more susceptible to convective instability. This result is robust and holds even for  $FO(1)$  as will be shown in the sequel.

## 5. Synergy between the two growth mechanisms

Having studied in the previous sections the limits isolating the two different energy growth mechanisms of perturbations in a stratified meridional shear flow, we now treat the general case in which growth occurs both due to downgradient Reynolds stresses and due to advection of zonal velocity. Consider first the case of a

wave with phase lines tilted with the shear in the horizontal ( $l/k < 0$ ). The solution is obtained by numerical integration of (8) in the absence of diffusion, and the energy evolution of the plane wave is given in terms of the Fourier amplitudes  $\hat{\xi}$ ,  $\hat{v}$ , and  $\hat{\rho}$  by

$$\hat{E} = \frac{1}{4(k^2 + m^2)} [|\hat{\xi}|^2 + K(t)^2 |\hat{v}|^2 + S(k^2 + m^2) |\hat{\rho}|^2]. \quad (29)$$

A typical energy evolution in the inviscid limit is shown in Fig. 5 for a three-dimensional perturbation with initial wavenumbers  $(k, l, m) = (1, -5, 10)$  and  $(k, l, m) = (1, -5, 50)$ . For  $m = 10$ , growth of zonal velocity due to advection, which is proportional to  $m/(l - kt)$ , is weak and energy evolution closely follows that predicted by (28) for  $(m/k) \ll S^{1/2}$ . For the case with  $m = 50$ , the oscillations shown in Fig. 5 are solely due to zonal velocity increase, indicating the presence of the roll mechanism. The oscillating behavior of the energy is due to wave interference, a consequence of the plane wave perturbations considered in this section. Because the meridional wavenumber is decreasing linearly with time in this case,  $m/(l - kt)$  decreases monotonically and rapidly, and the roll mechanism is important only during the early perturbation development, as illustrated by the decaying amplitude of oscillations with time. It is also worth noting that the oscillations are superposed on the energy increase due to Reynolds stresses alone, shown by the thick line, illustrating that the overall result is a superposition of the growth obtained by each of the mechanisms operating alone. Thus, zonal velocity and density amplifications occur independently, with the former being prevalent during the early stage of wave evolution and the latter for large times.

Consider now the case of waves with phase lines tilted against the shear in the horizontal ( $l/k > 0$ ). A typical energy evolution in the inviscid limit is shown in the middle of Fig. 5 for the example of initial wavenumbers  $(k, l, m) = (1, 5, 10)$ . The meridional wavenumber decreases linearly with time and becomes zero at  $t_v = l/k$ . We therefore expect the roll mechanism to be important for times  $t \sim t_v$ . For initial conditions  $[\hat{v}(0), \hat{\rho}(0)] = (1, 0)$ , amplification of  $u$  due to advection coincides with upgradient Reynolds stresses for  $t \sim t_v$ , leading to a further decay. For later times  $t > 2l/k$ , the wave leans with the shear,  $m/(l - kt)$  becomes small, resulting in a weak roll mechanism effect, and energy evolution is determined by the downgradient Reynolds stresses alone. However, in this case, gradual amplification after  $t > 2l/k$  is unable to compensate for the rapid loss at times  $t \sim t_v$ , and energy density is overall decreased. For

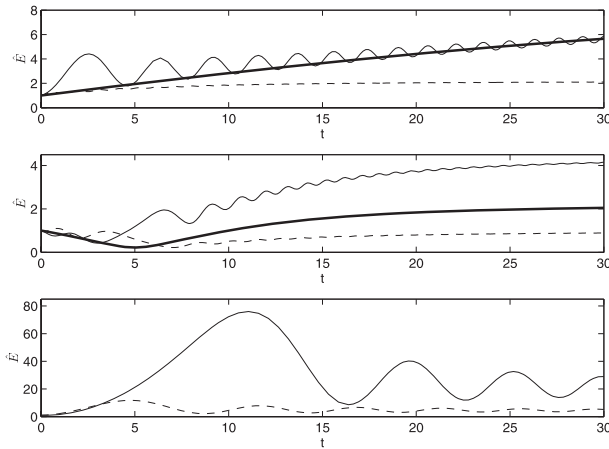


FIG. 5. (top) Energy evolution of a plane wave with  $(k, l, m) = (1, -5, 50)$  (solid line) and  $(k, l, m) = (1, -5, 10)$  (dashed line) as given by (29). The initial conditions are  $[\hat{v}(0), \hat{\rho}(0)] = (1, 0)$  and the static stability is  $S = 20$ . The energy evolution given by (28) for  $m = 50$  is also shown (thick line). The corresponding curve for  $m = 10$  coincides with the dashed line and is not shown. (middle) Energy evolution of a plane wave with  $(k, l, m) = (1, 5, 10)$  given by (29) for initial conditions  $[\hat{v}(0), \hat{\rho}(0)] = (1, 0.5)$  (solid line) and  $[\hat{v}(0), \hat{\rho}(0)] = (1, 0)$  (dashed line). Static stability is  $S = 20$  and the energy evolution given by (28) for  $m = 10$  is also shown (thick line). (bottom) Energy evolution of a plane wave with  $(k, l, m) = (1, 5, 25)$  (solid line) and  $(k, l, m) = (1, -5, 25)$  (dashed line) for initial conditions  $[\hat{v}(0), \hat{\rho}(0)] = (1, 0)$  and static stability  $S = 1$ . In all cases, the initial vorticity perturbation is such that the initial vertical component of potential vorticity is zero and the perturbation amplitude is normalized to yield unit initial energy.

$[\hat{v}(0), \hat{\rho}(0)] = (1, 0.5)$ , the Reynolds stresses near  $t \sim t_v$  are negative and amplification of  $u$  leads to a rapid energy density growth that is significantly enhanced at large times compared to the energy density growth arising only from the kinetic energy source associated with downgradient Reynolds stresses. Unlike in the case of a wave with phase lines tilted with the shear in the horizontal, in this case, with phase lines tilted against the shear, energy due to zonal velocity amplification is transferred through pressure work and buoyancy fluxes into the other velocity and density fields and about half of the amplified energy is in potential energy form. The resulting large density perturbations could potentially lead to convective instability.

The benefit from the synergism between downgradient Reynolds stresses and growth due to zonal advection is also evident for low values of static stability, for which the roll mechanism is stronger, as discussed in section 3. As illustrated in the bottom of Fig. 5, energy growth of waves with  $l/k > 0$  is larger than the corresponding energy growth of waves with opposite horizontal tilt ( $l/k < 0$ ), for which the two mechanisms are operating alone. In this case, though, only part of the amplified

zonal velocity is converted into density perturbations. This results in very large zonal velocity perturbations during the initial stage of evolution that decay with time as  $m/(l - kt)$  decreases monotonically. These perturbations could therefore lead to the formation of dynamically unstable regions if they persist long enough.

### 6. Optimal perturbations

#### a. Method of determining optimal perturbations

As discussed in the previous section, the roll mechanism and the Reynolds stresses and the synergy between them leads to amplification of zonal velocity or potential energy of plane wave perturbations that may result in breaking through shear or convective instability. It is therefore of interest to determine an upper bound for such transient amplifications and the initial perturbations yielding this growth. We thus calculate in this section the initial conditions yielding the largest growth of zonal velocity or density over a specified time interval  $T_{opt}$ . This optimization time,  $T_{opt}$ , is chosen using physical considerations, such as the time scale over which perturbation growth is limited by disruption due to turbulent fluctuations or by the initiation of breaking. Because we do not have a priori knowledge of this timescale, we chose it to be within a range of physically plausible values. A complete analysis proceeds from first using (9) [for  $\hat{q}(0) = 0$ ] to express  $\hat{\rho}$  in terms of  $\hat{\zeta}$  and  $\hat{v}$  and then writing (8a), (8b) in the compact form:

$$\frac{d\chi}{dt} = \mathbf{B}(t)\chi, \tag{30}$$

where  $\chi$  is the column vector  $\chi = [\hat{\zeta}, \hat{v}]^T$  and  $\mathbf{B}(t)$  is

$$\mathbf{B}(t) = \begin{bmatrix} \frac{kS(l - kt)}{k^2 + m^2} - \frac{K(t)^2}{\text{Re}} & -\frac{ik^2SK(t)^2}{m(k^2 + m^2)} - im \\ -\frac{imS(l - kt)^2}{(k^2 + m^2)K(t)^2} & \frac{2k(l - kt)}{K(t)^2} - \frac{kS(l - kt)}{k^2 + m^2} - \frac{K(t)^2}{\text{Re}} \end{bmatrix}.$$

The solution of (30) is given by  $\chi(t) = \Phi(t)\chi(0)$ , where  $\chi(0)$  is the initial state and  $\Phi(t)$  is the finite time propagator mapping the initial perturbation to its state at time  $t$ .

To address the possibility of dynamic and convective instability separately, we perform two optimization calculations. We seek the initial perturbation of unit energy leading to the largest growth in specified time  $T_{opt}$  of  $u^2$  and  $\rho^2$ , respectively. To achieve this, we define three positive definite matrices:

$$\mathbf{M}_0 = \frac{1}{4(k^2 + m^2)} \begin{bmatrix} 1 + \frac{Sl^2}{k^2 + m^2} & -\frac{ikS(k^2 + l^2 + m^2)l}{m(k^2 + m^2)} \\ \frac{ikS(k^2 + l^2 + m^2)l}{m(k^2 + m^2)} & (k^2 + l^2 + m^2) + \frac{k^2S(k^2 + l^2 + m^2)^2}{m^2(k^2 + m^2)} \end{bmatrix},$$

$$\mathbf{M}_u = \frac{1}{4(k^2 + m^2)^2} \begin{bmatrix} m^2 & -ikm(l - kt) \\ ikm(l - kt) & k^2(l - kt)^2 \end{bmatrix},$$

$$\mathbf{M}_\rho = \frac{S}{4(k^2 + m^2)^2} \begin{bmatrix} (l - kt)^2 & -\frac{ik(l - kt)K(t)^2}{m} \\ \frac{ik(l - kt)K(t)^2}{m} & \frac{k^2K(t)^4}{m^2} \end{bmatrix},$$

for which perturbation initial energy, square of zonal velocity, and potential energy are given by the Euclidean inner products:  $E(0) = \chi(0)^\dagger \mathbf{M}_0 \chi(0)$ ,  $(1/4)|\hat{u}(t)|^2 = \chi(0)^\dagger \mathbf{M}_u \chi(0)$ ,  $(S/4)|\hat{\rho}(t)|^2 = \chi(0)^\dagger \mathbf{M}_\rho \chi(0)$ , respectively, where  $\dagger$  denotes the complex conjugate.

For a given set of wavenumbers,  $(k, l, m)$ , singular-value decomposition of  $\mathbf{M}_i^{1/2} \Phi(T_{\text{opt}}) \mathbf{M}_0^{-1/2} = \mathbf{U}_i \mathbf{\Sigma}_i \mathbf{V}_i^\dagger$ , where  $i$  is either  $u$  or  $\rho$ ,  $\mathbf{U}_i$  and  $\mathbf{V}_i$  are unitary matrices, and  $\mathbf{\Sigma}_i$  is a diagonal matrix with positive elements ordered by growth, identifies the optimal perturbation  $\chi_{\text{opt}}$  as the first column of  $\mathbf{M}_0^{-1/2} \mathbf{V}_i$  (Farrell and Ioannou 1996). The square of the largest singular value is the largest of zonal velocity growth  $[(1/4)|\hat{u}_{\text{opt}}^{klm}(T_{\text{opt}})|^2]$  or potential energy growth  $[(S/4)|\hat{\rho}_{\text{opt}}^{klm}(T_{\text{opt}})|^2]$  (depending on the optimization) that can be achieved over the specified time interval  $T_{\text{opt}}$  by any initial plane wave of unit energy with wavenumbers  $(k, l, m)$ . The perturbation growing the most is then obtained numerically by a descent algorithm determining the wavenumbers  $(k, l, m)$ , maximizing  $(1/4)|\hat{u}_{\text{opt}}^{klm}(T_{\text{opt}})|^2$  or  $(S/4)|\hat{\rho}_{\text{opt}}^{klm}(T_{\text{opt}})|^2$ , and the corresponding growth is  $(1/4)|\hat{u}_{\text{max}}^2 = \max_{klm} [(1/4)|\hat{u}_{\text{opt}}^{klm}(T_{\text{opt}})|^2]$  and  $(S/4)|\hat{\rho}_{\text{max}}^2 = \max_{klm} [(S/4)|\hat{\rho}_{\text{opt}}^{klm}(T_{\text{opt}})|^2]$ , respectively.

### b. Growth and characteristics of optimal perturbations

Optimization calculations in this section are performed for a viscous flow, as viscosity prevents unrealistically small perturbations from emerging as optimals. Because there is no intrinsic space scale for an unbounded shear flow, the Reynolds number in this section is prescribed for a given coefficient of viscosity on perturbations having unit zonal wavenumber ( $k = 1$ ). Perturbations with larger zonal scale can be interpreted as evolving in a flow with a correspondingly higher Reynolds number.

The optimal growth for  $u$  and  $\rho$  as a function of optimizing time is shown in the left- and right-hand sides of Fig. 6, respectively, for static stability  $S = 1$  and  $S = 20$  and for  $\text{Re} = 10^4$  and  $\text{Re} = 10^6$ . Robust growth is found for both values of static stability, suggesting that waves can easily grow to breaking amplitude due to interaction with the mean flow. Low values of static stability favor zonal velocity growth, as the roll mechanism is stronger in this case, while amplification of density perturbations is larger for strongly stratified flows.

In all cases considered, the optimal perturbations have phase lines oriented against the shear in the horizontal ( $l/k > 0$ ) to benefit from the synergy between the two growth mechanisms. For large optimizing times, the optimal perturbations for zonal velocity growth have an initial horizontal tilt  $l/k \leq T_{\text{opt}}$  such that the plane wave assumes a cross-stream orientation ( $\tilde{l}/k = l/k - t = 0$ ) at a time  $t \leq T_{\text{opt}}$  to benefit from the synergy between downgradient Reynolds stresses and roll mechanisms occurring at  $t \sim l/k$ , and the initial energy is almost evenly distributed among  $u$ ,  $v$ ,  $w$ , and  $\rho$ . For small optimizing times,  $m/l$  is large and the initial energy is almost all in meridional velocity maximizing the benefit from growth due to advection of  $u$ .

On the other hand, the perturbations producing optimal density growth have an orientation utilizing the interplay between Reynolds stresses and advection of zonal velocity for transient growth while allowing enough time for the buoyancy fluxes to convert part of the kinetic energy growth attained to potential energy, as discussed in section 5. Therefore, their initial horizontal tilt  $l/k$  is rather small and weakly dependent on  $T_{\text{opt}}$ , such that kinetic energy amplification occurs early, while their orientation in the  $(y, z)$  plane is almost horizontal and the initial energy is predominantly in

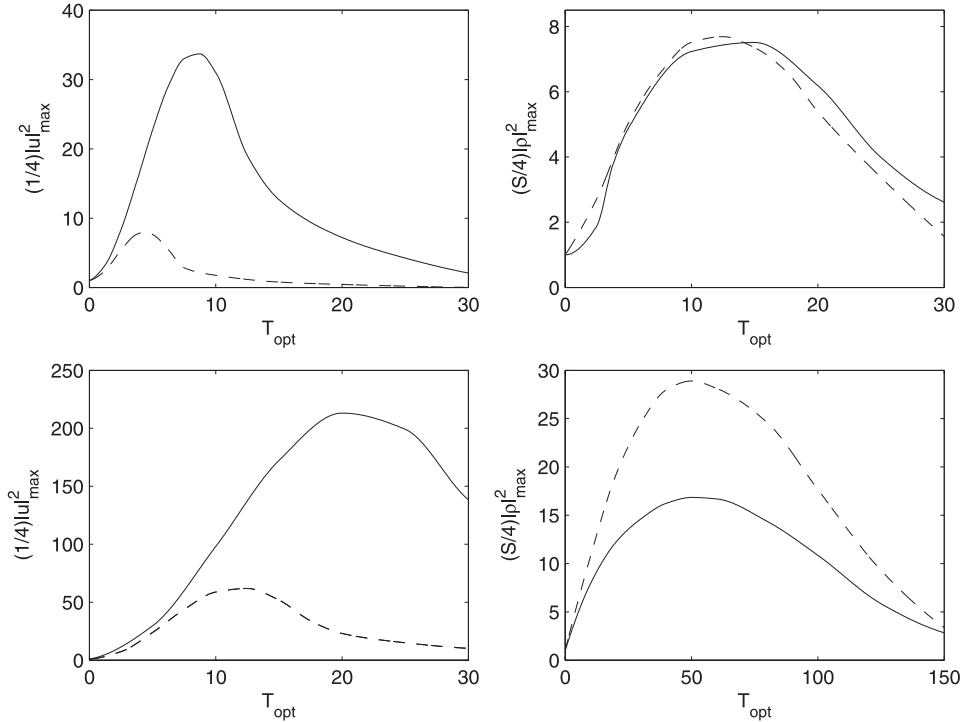


FIG. 6. (left) Optimal growth of zonal velocity  $(1/4)|u|_{\max}^2$  as a function of the optimization time  $T_{\text{opt}}$  for  $S = 1$  (solid line) and  $S = 20$  (dashed line) and for Reynolds number (top left)  $\text{Re} = 10^4$  and (bottom left)  $\text{Re} = 10^6$ . (right) Optimal growth of potential energy  $(S/4)|\rho|_{\max}^2$  as a function of the optimization time  $T_{\text{opt}}$  for  $S = 1$  (solid line) and  $S = 20$  (dashed line) and for Reynolds (top right) number  $\text{Re} = 10^4$  and (bottom right)  $\text{Re} = 10^6$ .

meridional velocity to benefit from the synergy of the two growth mechanisms.

**7. Growth of wave packets**

In this section we study the evolution of spatially localized wave packets to investigate whether the energy growth obtained depends sensitively on the wave interference that arises from plane wave solutions.

We consider a localized initial density and velocity perturbation of the form

$$[v(x, y, z, t = 0), \rho(x, y, z, t = 0)] = [A, 1]e^{ik_0x + im_0z + il_0y - (\delta y)^2}, \tag{31}$$

where  $\delta y$  defines the meridional extent of the perturbation and  $A$  is a chosen amplitude, and a vorticity perturbation

$$\zeta(x, y, z, t = 0) = \frac{i\delta y}{2m_0\sqrt{\pi}} \int_{-\infty}^{\infty} \frac{(m_0 + Ak_0)(k_0^2 + m_0^2) + Ak_0l^2}{l} e^{-\delta y^2(l-l_0)^2/4 + il_0y + ik_0x + im_0z} dl, \tag{32}$$

such that the initial potential vorticity is zero. This localized perturbation evolves as

$$[\zeta(x, y, z, t), v(x, y, z, t), \rho(x, y, z, t)] = \frac{1}{\sqrt{2\pi}} \int_{-\infty}^{\infty} [\hat{\zeta}(t), \hat{v}(t), \hat{\rho}(t)] e^{ik_0x + im_0z + i(l-k_0t)y} dl, \tag{33}$$

where  $[\hat{\zeta}(t), \hat{v}(t), \hat{\rho}(t)]$  are solutions to (8) (in the absence of diffusion) with initial conditions

$$[\hat{\zeta}(0), \hat{v}(0), \hat{\rho}(0)] = \left[ i \frac{(m_0 + Ak_0)(k_0^2 + m_0^2) + Ak_0l^2}{lm_0}, A, 1 \right] \times \frac{\delta y}{\sqrt{2}} e^{-\delta y^2(l-l_0)^2/4}, \tag{34}$$

whereas its energy evolves as

$$E = \frac{1}{8\pi(k_0^2 + m_0^2)} \int_{-\infty}^{\infty} \{ |\hat{\zeta}(t)|^2 + [k_0^2 + m_0^2 + (l - k_0t)^2] |\hat{v}(t)|^2 + S(k_0^2 + m_0^2) |\hat{\rho}(t)|^2 \} dl. \tag{35}$$

The initial conditions are such that the perturbations are localized and evolve as two counterpropagating wave packets. The wave packet amplitude is normalized to

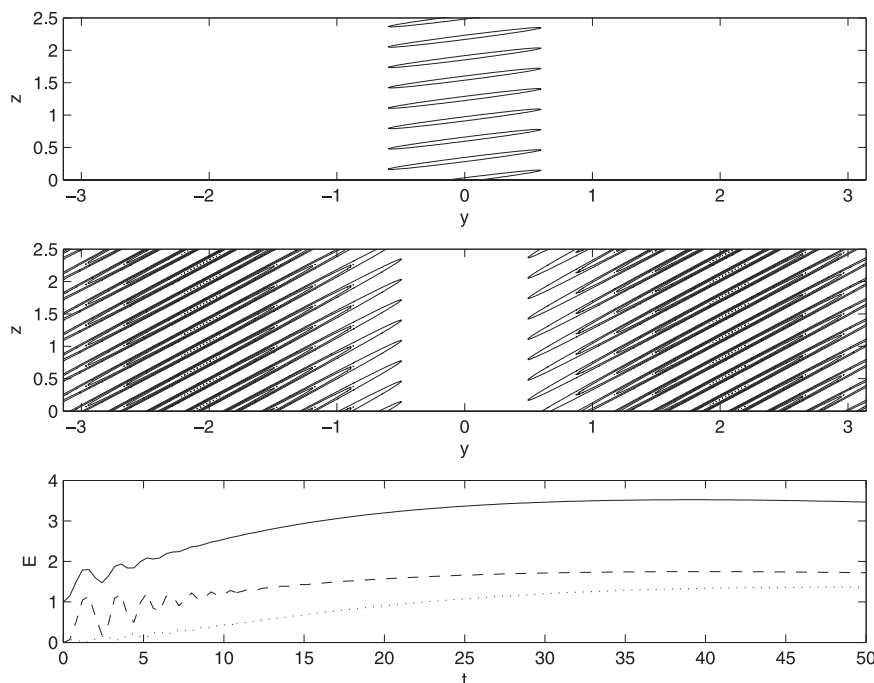


FIG. 7. Evolution of the wave packet given by (31), (32). The initial central wavenumber is  $(k_0, l_0, m_0) = (1, -5, 20)$ ,  $\delta y = 1.25$ ; the static stability is  $S = 20$  and  $A = 20$ . Snapshots of density at (top)  $t = 0$  and (middle)  $t = 16$ . The contour interval is 0.06. (bottom) Evolution of energy (solid line), potential energy (dashed line), and  $(1/4)|w|^2$  (dotted line).

yield unit initial energy, and the evolution is calculated using numerical quadrature of the Fourier integrals (33), (35).

We first choose static stability  $S = 20$  and a central wavenumber  $(k_0, l_0, m_0) = (1, -5, 20)$ , such that the two growth mechanisms operate independently ( $l_0/k_0 < 0$ ). Evolution of this localized perturbation in a vertical  $(y, z)$  plane is illustrated in Fig. 7, where contours of density perturbation at successive times are shown. As the wave packets propagate toward their trapping levels located at  $y = \pm 3.4$ , the meridional wavenumber decreases resulting in phase lines tilting toward the vertical. The bottom of Fig. 7 shows the evolution of wave packet energy. Wave interference is only evident during the initial stage of evolution before wave packets become separated in space. The growth due to Reynolds stresses is maximized when the wave packet has almost reached its trapping level and is partitioned between potential energy and  $(1/4)|w|^2$ , a behavior that was also found by Staquet and Huerre (2002) in their direct numerical simulation experiment of an inertia-gravity wave packet approaching a finite shear layer. The large amplification of density in their simulation resulted in convective overturning, showing the importance of the linear growth mechanism due to Reynolds stresses studied in this work.

To study the evolution of waves tilted against the shear, we choose a central wavenumber  $(k_0, l_0, m_0) = (1, 5, 20)$ . The wave packets that are initially localized around  $y = 0$  (Fig. 8a) propagate toward their turning levels located at  $y = \pm 0.8$ . Their meridional wavenumber decreases and the phase lines assume a horizontal orientation (Fig. 8b). After reaching the turning level, the meridional wavenumber changes sign and the phase line tilt increases in the opposite direction (Fig. 8c), while they propagate toward their trapping levels located at  $y = \pm 3.4$ . The wave packet energy evolution shown in Fig. 8d is similar to that found for waves tilted with the shear (Fig. 7), reaching, however, larger values due to synergy between the roll mechanism and Reynolds stress mechanism in this case.

The energy evolution for  $S = 1$  is shown in Fig. 9 for waves tilted with and against the shear. In this case, the turning and trapping levels are located close to the initial position of the wave packet, and wave interference is evident even for such localized perturbations. Phase line orientation is initially almost horizontal (large  $m_0$ ), leading to a large amplification of zonal velocity due to roll advection that dominates the observed growth and might lead to shear instability. Further investigation is needed to determine if the induced shear persists long enough in the nonlinear regime for small perturbations

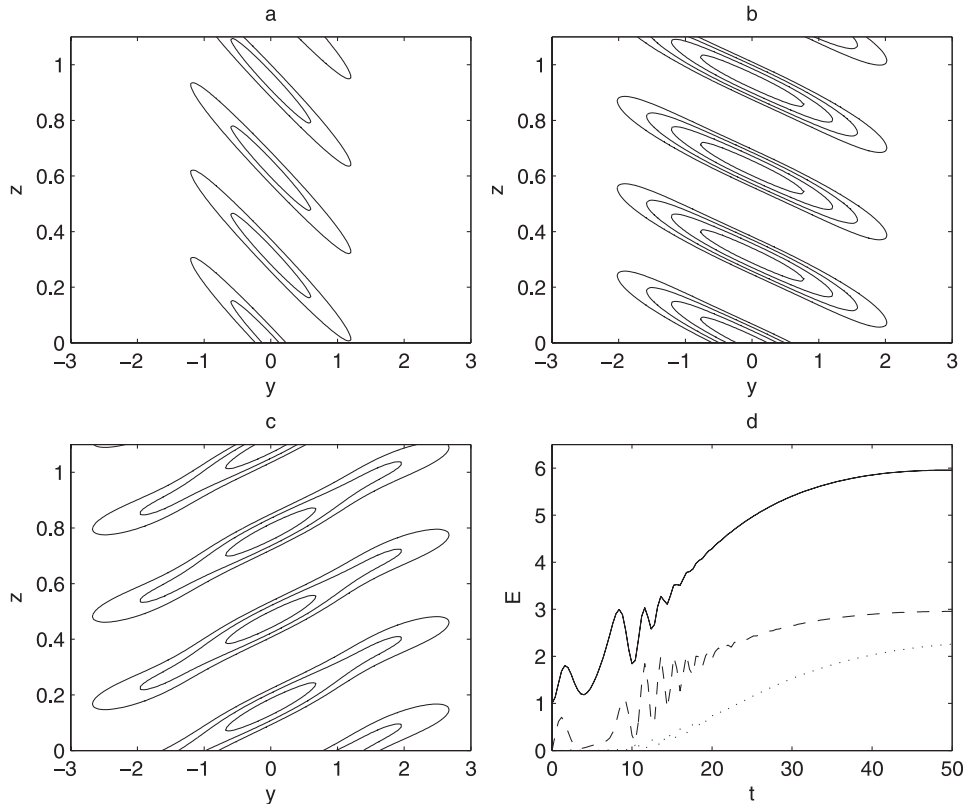


FIG. 8. Evolution of the wave packet given by (31), (32). The initial central wavenumber is  $(k_0, l_0, m_0) = (1, 5, 20)$ ,  $\delta y = 1.25$ ; the static stability is  $S = 20$  and  $A = 20$ . Snapshots of density at (a)  $t = 0$ , (b)  $t = 2.4$ , and (c)  $t = 6$ . The contour interval is 0.03. (d) Evolution of energy (solid line), potential energy (dashed line), and  $(1/4)|w|^2$  (dotted line).

to grow and destroy wave packet coherence. This investigation is part of ongoing research.

### 8. Conclusions

Interaction of internal gravity waves with a horizontal shear flow for perturbations with zero potential vorticity was investigated making use of closed-form solutions.

Zonally independent ( $k = 0$ ) solutions were found to propagate in the  $(y, z)$  plane with a constant group velocity and to grow due to advection of zonal velocity. The resulting growth of zonal velocity was found to be proportional to the tilt of constant phase lines in the  $(y, z)$  plane,  $m/l$ , and inversely proportional to the square of static stability. The initial conditions yielding the optimal growth were found to be velocity perturbations.

On the other hand, meridional propagation of perturbations for  $F = (m/k)S^{1/2} \ll 1$  is limited by turning levels where the waves are reflected, and trapping levels where the waves stagnate. In this case, perturbations amplify due to the kinetic energy source associated with

downgradient Reynolds stresses. Almost all of the energy growth obtained is partitioned between potential energy and kinetic energy associated with the vertical velocity.

For  $F = O(1)$ , the interplay between the two growth mechanisms was found to produce large and robust amplification of either zonal velocity or both density and vertical velocity, potentially leading to shear or convective instability, respectively. Waves with phase lines tilted against the shear in the horizontal ( $l/k > 0$ ) benefit more from this synergy and reach larger amplitudes compared to opposite tilted waves ( $l/k < 0$ ). For large static stability, robust amplification of density and vertical velocity occurs for localized wave packets with moderate values of  $m/k$  and could result in convective breaking near the trapping level, as found by Staquet and Huerre (2002), who studied breaking of wave packets in nonlinear simulations. For lower static stability, the possibility of shear instability arises, especially for waves with large  $m/k$ , due to the large amplification in zonal velocity during the early stages of evolution. In this case, breaking is expected near the

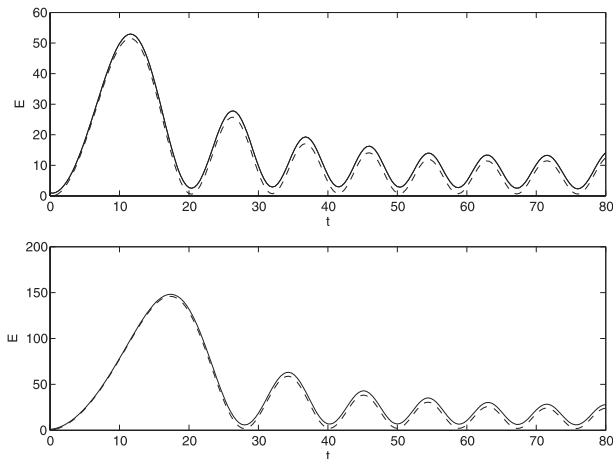


FIG. 9. Evolution of total energy (solid line) and the zonal energy component  $(1/4)ll^2$  (dashed line) for an initial wave packet with initial central wavenumber (top)  $(k_0, l_0, m_0) = (1, -5, 100)$  and (bottom)  $(k_0, l_0, m_0) = (1, 5, 100)$  as given by (31), (32). The static stability is  $S = 1$ ,  $\delta y = 1.25$ , and  $A = 40$ .

turning level for waves with phase lines tilted initially against the shear ( $ll/k > 0$ ) or during the early stages of propagation for waves with  $ll/k < 0$ .

Rotation and nonlinear processes affect the long-term behavior of wave packets, and therefore nonlinear calculations on an  $f$  plane are needed to determine the robustness of the linear growth mechanisms considered in this work. Nevertheless, qualitative agreement of our results with the results of Staquet and Huerre's (2002) direct numerical simulation of a breaking wave packet on an  $f$  plane, as well as previous studies such as that of Jacobitz and Sarkar (1998), who found that turbulence production in a stably stratified fluid is strongly increased when the flow involves a horizontally sheared mean flow, suggests that these linear mechanisms play a significant role in wave breaking and mixing.

*Acknowledgments.* The authors thank two anonymous reviewers for their useful comments and numerous suggestions, which helped to improve the manuscript. This research was supported by NSF ATM-0736022.

## APPENDIX A

### Optimal Zonally Independent Perturbations

The inviscid, zonally independent perturbations leading to the largest energy growth over a specified time interval within the initial stage of wave interference are obtained by following the method outlined in section 6 and expressing (30) in terms of the new variable  $\mathbf{y} = \mathbf{M}_{k0}^{1/2}\boldsymbol{\chi}$ , where  $\mathbf{M}_{k0}$  is the energy metric

$$\mathbf{M}_{k0} = \frac{1}{4m^2} \begin{pmatrix} 1 + Sl^2/m^2 & 0 \\ 0 & l^2 + m^2 \end{pmatrix},$$

for which perturbation energy is given by the inner product:  $E = \mathbf{y}^\dagger \mathbf{y}$ . In this variable, the governing equations are transformed to

$$\frac{d\mathbf{y}}{dt} = \mathbf{D}_0 \mathbf{y}, \quad (\text{A1})$$

where  $\mathbf{D}_0$  is

$$\mathbf{D}_0 = \mathbf{M}_{k0}^{1/2} \mathbf{B} \mathbf{M}_{k0}^{-1/2} = \begin{pmatrix} 0 & -ib \\ -i\omega_0^2/b & 0 \end{pmatrix},$$

$\omega_0$  is given by (17), and  $b = \sqrt{m^2 + l^2 S} / \sqrt{l^2 + m^2}$ . The solution of (A1) is  $\mathbf{y}(t) = e^{\mathbf{D}_0 t} \mathbf{y}(0)$ , where

$$e^{\mathbf{D}_0 t} = \begin{bmatrix} \cos(\omega_0 t) & -ib \sin(\omega_0 t) / \omega_0 \\ -i\omega_0 \sin(\omega_0 t) / b & \cos(\omega_0 t) \end{bmatrix}$$

is the propagator. The optimal perturbation leading to the largest energy growth over a specified time interval  $t = T_{\text{opt}}$  can be identified as the eigenvector corresponding to the largest eigenvalue of  $\mathbf{P} = e^{\mathbf{D}_0^\dagger T_{\text{opt}}} e^{\mathbf{D}_0 T_{\text{opt}}}$  (Farrell and Ioannou 1996). Eigenanalysis of  $\mathbf{P}$  reveals that the largest eigenvalue, corresponding to the optimal growth, is

$$\begin{aligned} E_{\text{opt}}^{lm} &= \cos^2(\omega_0 T_{\text{opt}}) + \frac{b^4 + \omega_0^4}{2b^2\omega_0^2} \sin^2(\omega_0 T_{\text{opt}}) \\ &+ \frac{1}{2} \sqrt{\left[ 2\cos^2(\omega_0 T_{\text{opt}}) + \frac{b^4 + \omega_0^4}{b^2\omega_0^2} \sin^2(\omega_0 T_{\text{opt}}) \right]^2 - 4} \\ &= 1 + \frac{m^4 \sin^2(\omega_0 T_{\text{opt}})}{2l^2 S(l^2 S + m^2)} \\ &+ \sqrt{\frac{m^8 \sin^4(\omega_0 T_{\text{opt}})}{4l^4 S^2(l^2 S + m^2)^2} + \frac{m^4 \sin^2(\omega_0 T_{\text{opt}})}{l^2 S(l^2 S + m^2)}}. \quad (\text{A2}) \end{aligned}$$

The optimal growth increases with  $m/l$  and asymptotically approaches  $\sigma \rightarrow 1 + T_{\text{opt}}^2$  for  $m/l \rightarrow \infty$ . Therefore, the optimal perturbations are confined in the horizontal plane and can be readily shown to be velocity perturbations  $[\hat{\rho}(0)O(llm) \ll 1]$ .

To find the optimal perturbations leading to the largest energy growth during the stage of wave spatial separation, we solve the following optimization problem: we seek the initial perturbations maximizing the energy of both waves in the stage of wave spatial separation, which is given by

$$E_s = \frac{1}{8} \left[ \frac{m^2 + 2l^2 S}{l^2} |\hat{\rho}(0)|^2 + \frac{(l^2 + m^2)(m^2 + 2l^2 S)}{m^2 l^2 S} |\hat{v}(0)|^2 \right],$$

$$\hat{\rho}(l, t) = \sqrt{\omega(t)} \hat{\rho}_0(l) [A_+(l) e^{i\sqrt{S} \int_0^t \omega(s) ds} + A_-(l) e^{-i\sqrt{S} \int_0^t \omega(s) ds}], \tag{B1}$$

given the constrain of unit initial energy

$$E(0) = \frac{1}{4m^2} \left[ \frac{m^2(l^2 S + m^2)}{l^2} |\hat{\rho}(0)|^2 + (l^2 + m^2) |\hat{v}(0)|^2 \right].$$

Using the method of Lagrangian multipliers, we find that the optimal growth increases with  $m/l$  in this case as well. For  $m/l \gg 1$ , the optimal perturbation has  $\hat{\rho}(0) \simeq 0$ , yielding a maximal growth  $E_{opt}^{lm} = 1 + m^2/(2l^2 S)$  that is independent of the optimization time.

APPENDIX B

**Propagation of Wave Packets in Stratified Shear Flow**

Consider the initial wave packet given by (31)–(32), where the width of the wave packet  $\delta y \gg 1$  is such that it consists of wave vectors  $\Delta l$  around the central vector  $l_0$  in wavenumber space. The evolution of this localized perturbation is given by (33), where  $\hat{\rho}(l, t)$  is a solution to (10) (in the absence of diffusion) with initial conditions

$$\left[ \hat{\rho}(0), \frac{d\hat{\rho}}{dt}(0) \right] = \left[ \hat{\rho}_0(l), \frac{ik_0}{k_0^2 + m_0^2} \hat{\xi}_0(l) - \frac{m_0 l}{k_0^2 + m_0^2} \hat{v}_0(l) \right],$$

where  $[\hat{\rho}_0(l), \hat{\xi}_0(l), \hat{v}_0(l)]$  are given by (34), and  $\hat{\xi}(t), \hat{v}(t)$  can be determined from  $\hat{\rho}(t)$  using (8c) and (9). For  $(m/k) \ll S^{1/2}$ , Eq. (10) accepts the following WKB solution:

where

$$A_{\pm}(l) = \frac{1}{2\sqrt{\omega(0)}} \left\{ 1 \pm \frac{i[k_0 m_0 + A(k_0^2 + l^2)]}{m_0 l \omega(0) \sqrt{S}} \right\},$$

yielding the following evolution of the density field:

$$\rho(x, y, z, t) = \frac{1}{\sqrt{2\pi}} \int_{-\infty}^{\infty} \hat{\rho}_0(l) \sqrt{\omega(t)} [A_+(l) e^{i\sqrt{S} \int_0^t \omega(s) ds} + A_-(l) e^{-i\sqrt{S} \int_0^t \omega(s) ds}] e^{ik_0 x + im_0 z + i(l-k_0 t)y} dl.$$

Expanding all functions near  $l_0$ , yields

$$\rho(x, y, z, t) = \frac{\delta y e^{ik_0 x + im_0 z}}{2\sqrt{\pi}} \int_{-\infty}^{\infty} e^{-\tilde{l}^2 \delta y^2 / 4} [\sqrt{\omega(l_0, t)} + \partial_{\tilde{l}} \sqrt{\omega(l, t)}|_{l_0} (l - l_0) + \dots] (G_+ + G_-) d\tilde{l}, \tag{B2}$$

where

$$G_{\pm} = [A_{\pm}(l_0) + \partial_{\tilde{l}} A_{\pm}|_{l_0} (l - l_0) + \dots] \times e^{i(l_0 - k_0 t)y + i(l - l_0)y \pm i\sqrt{S} \int_0^t [\omega(l_0, s) + \partial_{\tilde{l}} \omega(l, s)|_{l_0} (l - l_0) + \dots] ds}.$$

Changing variables  $\tilde{l} = l - l_0$ , Eq. (B2) becomes at leading order

---


$$\begin{aligned} \rho(x, y, z, t) &= \frac{\delta y A_+(l_0) \sqrt{\omega(l_0, t)} e^{ik_0 x + im_0 z + i(l_0 - k_0 t)y + i\sqrt{S} \int_0^t \omega(l_0, s) ds}}{2\sqrt{\pi}} \int_{-\infty}^{\infty} e^{-\tilde{l}^2 \delta y^2 / 4} e^{i\tilde{l} [y + i\sqrt{S} \int_0^t \partial_{\tilde{l}} \omega(l, s)|_{l_0}]} d\tilde{l} \\ &+ \frac{\delta y A_-(l_0) \sqrt{\omega(l_0, t)} e^{ik_0 x + im_0 z + i(l_0 - k_0 t)y - i\sqrt{S} \int_0^t \omega(l_0, s) ds}}{2\sqrt{\pi}} \int_{-\infty}^{\infty} e^{-\tilde{l}^2 \delta y^2 / 4} e^{i\tilde{l} [y - i\sqrt{S} \int_0^t \partial_{\tilde{l}} \omega(l, s)|_{l_0}]} d\tilde{l} \\ &= \sqrt{\omega(l_0, t)} A_+(l_0) e^{-ik_0 y t + i\sqrt{S} \int_0^t [\omega(l_0, s) - l_0 \partial_{\tilde{l}} \omega(l, s)|_{l_0}] ds} \rho \left( x, y + \sqrt{S} \int_0^t \partial_{\tilde{l}} \omega(l, s)|_{l_0} ds, z, t = 0 \right) \\ &+ \sqrt{\omega(l_0, t)} A_-(l_0) e^{-ik_0 y t - i\sqrt{S} \int_0^t [\omega(l_0, s) - l_0 \partial_{\tilde{l}} \omega(l, s)|_{l_0}] ds} \rho \left( x, y - \sqrt{S} \int_0^t \partial_{\tilde{l}} \omega(l, s)|_{l_0} ds, z, t = 0 \right) \\ &= \sqrt{\omega(l_0, t)} A_+(l_0) e^{-ik_0 y t + i\sqrt{S} \int_0^t [\omega(l_0, s) - l_0 \partial_{\tilde{l}} \omega(l, s)|_{l_0}] ds} \rho(x, y + \sqrt{S} [\omega(l_0, t) - \omega(l_0, 0)] / k_0, z, t = 0) \\ &+ \sqrt{\omega(l_0, t)} A_-(l_0) e^{-ik_0 y t - i\sqrt{S} \int_0^t [\omega(l_0, s) - l_0 \partial_{\tilde{l}} \omega(l, s)|_{l_0}] ds} \rho(x, y - \sqrt{S} [\omega(l_0, t) - \omega(l_0, 0)] / k_0, z, t = 0). \end{aligned}$$

So the solution consists of two wave packets propagating toward opposite directions according to (25) and with group velocity given by (26), where the plus and minus signs correspond to the first and second terms, respectively.

The perturbation's energy is given by (35), in which the Fourier amplitudes  $\hat{\zeta}(t), \hat{v}(t)$  can be obtained in terms of  $\hat{\rho}(t)$ , using (8c) and (9), and for  $(m/k) \ll S^{1/2}$  they are

$$[\hat{\zeta}(t), \hat{v}(t)] = \left[ \frac{k}{\omega(t)}, -\frac{im\omega(t)(l-kt)}{k^2 + (l-kt)^2} \right] S^{1/2} \hat{\rho}(t),$$

yielding an overall energy

$$E = \frac{S}{4\pi} \int_{-\infty}^{\infty} |\hat{\rho}(t)|^2 dt. \quad (\text{B3})$$

Introducing (B1) into (B3) and expanding the integrand near  $l_0$  readily shows that this leads to the energy growth for each of the wave packets given by (28).

#### REFERENCES

- Badulin, S. I., and V. I. Shrira, 1993: On the irreversibility of internal wave dynamics due to wave trapping by flow inhomogeneities. Part I: Local analysis. *J. Fluid Mech.*, **251**, 21–53.
- , V. M. Vasilenko, and N. N. Golenko, 1990: Transformation of internal waves in the equatorial Lemonosov current. *Izv. Atmos. Oceanic Phys.*, **26**, 110–117.
- Bakas, N. A., and B. F. Farrell, 2009: Gravity waves in a horizontal shear flow. Part II: Interaction between gravity waves and potential vorticity perturbations. *J. Phys. Oceanogr.*, **39**, 497–511.
- , P. J. Ioannou, and G. E. Kefaliakos, 2001: The emergence of coherent structures in stratified shear flow. *J. Atmos. Sci.*, **58**, 2790–2806.
- Bretherton, F. P., 1966: The propagation of groups of internal gravity waves in a shear flow. *Quart. J. Roy. Meteor. Soc.*, **92**, 466–480.
- Brown, S. N., and K. Stewartson, 1982: On the nonlinear reflection of a gravity wave at a critical level. Part III. *J. Fluid Mech.*, **113**, 215–250.
- Ellingsen, T., and E. Palm, 1975: Stability of linear flow. *Phys. Fluids*, **18**, 487–488.
- Erokhin, N. S., and R. S. Sagdeev, 1985: On the theory of anomalous focusing of internal waves in a two-dimensional non-uniform fluid. Part II: Precise solution of the two-dimensional problem with regard to viscosity nonstationarity. *Morsk. Gidrofiz. J.*, **4**, 3–10.
- Farrell, B. F., and P. J. Ioannou, 1993: Optimal excitation of three-dimensional perturbations in viscous constant shear flow. *Phys. Fluids A*, **5**, 1390–1400.
- , and —, 1996: Generalized stability theory. Part I: Autonomous operators. *J. Atmos. Sci.*, **53**, 2025–2040.
- Frankignoul, C. J., 1974: Observed anisotropy of spectral characteristics of internal waves induced by low-frequency currents. *J. Phys. Oceanogr.*, **4**, 625–634.
- Garrett, C., and W. Munk, 1979: Internal waves in the ocean. *Annu. Rev. Fluid Mech.*, **11**, 339–369.
- Gregg, M. C., 1989: Scaling turbulent dissipation in the thermocline. *J. Geophys. Res.*, **94** (C7), 9686–9698.
- Ivanov, Y. A., and Y. G. Morozov, 1974: Deformation of internal gravity waves by a stream with horizontal shear. *Oceanology*, **14**, 457–461.
- Jacobitz, F. G., and S. Sarkar, 1998: The effect of nonvertical shear on turbulence in a stably stratified medium. *Phys. Fluids*, **10**, 1158–1168.
- Kalashnik, M. V., G. R. Mamatsashvili, G. D. Chagelishvili, and J. G. Lominadze, 2006: Linear dynamics of non-symmetric perturbations in geostrophic horizontal shear flows. *Quart. J. Roy. Meteor. Soc.*, **132**, 505–518.
- Landahl, M. T., 1980: A note on an algebraic instability of inviscid parallel shear flows. *J. Fluid Mech.*, **98**, 243–253.
- Miropol'skiy, Y. Z., 1974: Propagation of internal waves in an ocean with horizontal density field inhomogeneities. *Izv. Atmos. Oceanic Phys.*, **10**, 312–318.
- Moffat, H. K., 1967: The interaction of turbulence with strong shear. *Atmospheric Turbulence and Radio Wave Propagation*, A. M. Yaglom and V. I. Tatarsky, Eds., Nauka, 139–161.
- Olbers, D. J., 1981: The propagation of internal waves in a geostrophic current. *J. Phys. Oceanogr.*, **11**, 1224–1233.
- Phillips, O.M., 1966: *The Dynamics of the Upper Ocean*. Cambridge University Press, 366 pp.
- Ruddick, B. R., and T. M. Joyce, 1979: Observation of the interaction between the internal wave field and low-frequency flows in the North Atlantic. *J. Phys. Oceanogr.*, **9**, 498–517.
- Samodurov, A. Z., 1974: Internal waves in a medium with a horizontally varying Brunt-frequency. *Izv. Atmos. Oceanic Phys.*, **10**, 185–191.
- Staquet, C., and G. Huerre, 2002: Transport across a barotropic shear flow by breaking inertia gravity waves. *Phys. Fluids*, **14**, 1993–2006.
- , and J. Sommeria, 2002: Internal gravity waves: From instabilities to turbulence. *Annu. Rev. Fluid Mech.*, **33**, 559–593.
- Sutherland, B. R., 2000: Internal wave reflection in uniform shear. *Quart. J. Roy. Meteor. Soc.*, **126**, 3255–3286.
- Thorpe, S. A., 1981: An experimental study of critical layers. *J. Fluid Mech.*, **103**, 321–344.